Rate Constants and Hydrogen Isotope Substitution Effects in the $CH_3 + HCl$ and $CH_3 + Cl_2$ Reactions

Arkke J. Eskola,[†] Raimo S. Timonen,[†] Paul Marshall,[‡] Evgeni N. Chesnokov,[§] and Lev N. Krasnoperov*,[||]

Laboratory of Physical Chemistry, P.O. Box 55, FIN-00014 University of Helsinki, Finland, Department of Chemistry, University of North Texas, P.O., Box 305070, Denton, Texas 76203-5070, Institute of Chemical Kinetics and Combustion, Institutskaya 3, Novosibirsk, 630090, Russia, and Department of Chemistry and Environmental Science, New Jersey Institute of Technology, Newark, New Jersey 07102

Received: March 6, 2008; Revised Manuscript Received: June 4, 2008

The kinetics of the $CH_3 + Cl_2$ (k_{2a}) and $CD_3 + Cl_2$ (k_{2b}) reactions were studied over the temperature range 188−500 K using laser photolysis−photoionization mass spectrometry. The rate constants of these reactions are independent of the bath gas pressure within the experimental range, 0.6−5.1 Torr (He). The rate constants were fitted by the modified Arrhenius expression, $k_{2a} = 1.7 \times 10^{-13}(T/300\ \mathrm{K})^{2.52}\exp(5520\ \mathrm{J\ mol^{-1}/RT})$ and $k_{2b} = 2.9 \times 10^{-13}(T/300\ \mathrm{K})^{1.84}\exp(4770\ \mathrm{J\ mol^{-1}/RT})\ \mathrm{cm^3\ molecule^{-1}\ s^{-1}}$. The results for reaction 2a are in good agreement with the previous determinations performed at and above ambient temperature. Rate constants of the $CH_3 + Cl_2$ and $CD_3 + Cl_2$ reactions obtained in this work exhibit *minima* at about 270−300 K. The rate constants have positive temperature dependences above the minima, and negative below. Deuterium substitution increases the rate constant, in particular at low temperatures, where the effect reaches ca. 45% at 188 K. These observations are quantitatively rationalized in terms of stationary points on a potential energy surface based on QCISD/6−311G(d,p) geometries and frequencies, combined with CCSD(T) energies extrapolated to the complete basis set limit. 1D tunneling as well as the possibility of the negative energies of the transition state are incorporated into a transition state theory analysis, an approach which also accounts for prior experiments on the $CH_3 + HCl$ system and its various deuterated isotopic substitutions [Eskola, A. J.; Seetula, J. A.; Timonen, R. S. *Chem. Phys.* **2006**, *331*, 26].

Introduction

Kinetics of reactions of small hydrocarbon free radicals with hydrogen halides and halogens is of great importance for the thermochemistry of hydrocarbons as well as for fundamental understanding of the reaction dynamics.[1,2] Bond energy determinations require knowledge of the equilibrium constants, which are determined by combining the forward and the reverse rate constants. Usually, the rate constants are fitted by Arrhenius expressions, which consequently are used to derive the equilibrium constants. This approach assumes linearity of the Arrhenius plots, which is not a critical assumption provided that both rate constants are measured over the same temperature range. However, because of the experimental limitations, the rate constants for the forward and reverse reactions are often determined over different temperature ranges. As a result, possible deviations from the linear Arrhenius dependence becomes a critical issue, and accurate temperature dependences are required for reliable data fitting and extrapolation.

Many reactions that are used in thermochemical studies exhibit complicated temperature dependences, such as curved Arrhenius plots and negative temperature dependences.[3–9] For some reactions that exhibit negative temperature dependences at low temperatures, theoretical calculations predict inversion of the temperature dependence from positive at elevated temperatures to negative at low temperatures.[10,11] A recent experimental study on the kinetics of reactions of methyl radical with hydrogen chloride and the deuterium-substituted isotopomers (reactions 1a−d) revealed strongly curved Arrhenius plots:[12]

$$CH_3 + HCl \rightarrow CH_4 + Cl \quad (1a)$$

$$CD_3 + HCl \rightarrow CD_3H + Cl \quad (1b)$$

$$CH_3 + DCl \rightarrow CH_3D + Cl \quad (1c)$$

$$CD_3 + DCl \rightarrow CD_4 + Cl \quad (1d)$$

In the current experimental study, a small negative temperature dependence was found in the reactions of methyl radical and its deuterated analogue with molecular chlorine:

$$CH_3 + Cl_2 \rightarrow CH_3Cl + Cl \quad (2a)$$

$$CD_3 + Cl_2 \rightarrow CD_3Cl + Cl \quad (2b)$$

Theoretical calculations performed at the coupled cluster level were combined with transition state theory including 1D tunneling corrections. For reaction 1, good agreement with the experiments was obtained at elevated temperatures for all isotopomers without any adjustments of the parameters of the theoretical potential energy surface. The strong curvature of the Arrhenius plots has been unambiguously assigned to the tunneling, and a reasonable agreement with the experiment was achieved using 1D-tunneling with a truncated parabolic potential based on the harmonic imaginary frequencies of the transition state. For reaction 2, it was found that either slight reduction of

* Author to whom correspondence should be addressed. Fax: (973)-596-3586; e-mail: krasnoperov@adm.njit.edu.
[†] University of Helsinki.
[‡] University of North Texas.
[§] Institute of Chemical Kinetics and Combustion.
[||] New Jersey Institute of Technology.

10.1021/jp801999w CCC: $40.75
Published on Web 07/23/2008

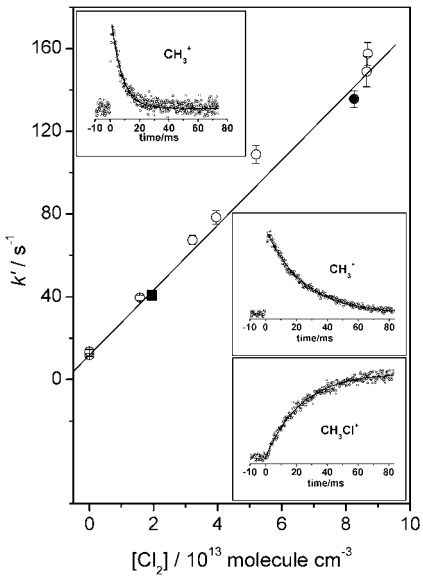

Figure 1. Plot of the pseudo-first-order CH_3 decay rate constant k' vs $[Cl_2]$ at $T = 188$ K and $p = 1$ Torr employing the 17 mm i.d. reactor tube. The insert in the upper left corner shows the profile for the CH_3 decay which corresponds to the solid circle in the plot: $k'_{decay}(CH_3) = 135 \pm 4\ s^{-1}$ and $k_0 = 12 \pm 1\ s^{-1}$. The inserts in the lower right corner show profiles for the CH_3 radical signal decay and product (CH_3Cl) formation that correspond to the solid square: $k'_{decay}(CH_3) = 41 \pm 1\ s^{-1}$ and $k'_{rise}(CH_3Cl) = 43 \pm 1\ s^{-1}$. Uncertainties are one standard deviation (1σ).

the barrier energy within the probable accuracy of the theory (by 0.9 kJ mol^{-1}) or/and usage of the imaginary frequency on the "vibrationally adiabatic" potential energy surface bring the theory in reasonable agreement with the experiment. For this reaction, the theoretical barriers are small, and the adjusted barrier for reaction 2b has a negative energy relative to the reactants; therefore, the modified transition state theory (MTST[11,13]) was used to interpret the experimental observations.

Experimental Section

Details of the experimental apparatus used in this study have been described in detail previously;[14] therefore, only a brief overview is given here. The methyl radicals R ($R = CH_3$ or CD_3) were generated using photolysis of appropriate precursors along the flow reactor by unfocused 193 nm light from a pulsed exciplex ArF laser (ELI-76E). The gas mixture flowing through the tubular, temperature-controlled reactor coupled with a photoionization mass spectrometer (PIMS) contained the radical precursor (<0.10%), Cl_2 in varying amounts (<0.5%) and an inert carrier gas (He) in large excess (>99.4%). The employed reactors were made of seamless stainless steel or Pyrex-glass tubes with 8 or 17 mm inner diameters (i.d.). The reactors were coated with poly(dimethylsiloxane) 200 fluid (8 mm tube) and halocarbon wax (17 mm tube), respectively. The linear gas velocities at pressures used of 0.5−8 Torr and temperatures in the range 188−500 K were typically about 4−6 m s^{-1} inside the reactor, which implies that the gas mixture passed through the uniformly cooled (heated) zone in about 80 ms. The gas was continuously sampled through a 0.4 mm diameter hole in the side wall of the reactor and formed into a beam by a conical skimmer before it entered a vacuum chamber containing the PIMS. As the gas beam traversed the ion source, a portion was selectively photoionized and the ions formed were mass selected in a quadrupole mass spectrometer (Extrel, C-50/150-QC/19 mm rods). The selected ions were detected by an off-axis electron multiplier.

Ionizing radiation in the PIMS was provided by a Cl-lamp (8.9−9.1 eV) for 2,4-hexadiene, a H-lamp (10.2 eV) for CD_3, CH_3, $CD_3C(O)CD_3$, and $CH_3C(O)CH_3$, and an Ar-lamp (11.6−11.8 eV) for CH_3NO_2 and CH_3Cl. Temporal ion signals were recorded by a multichannel scaler (EG&G Ortec MCS plus) from 10 ms before each laser pulse up to 80 ms following the pulse. All measurements were performed at the initial concentrations of the stable reactant in large excess of the free radical species (the pseudo-first-order conditions). Typically, a profile from 3000−10000 repetitions was accumulated at about 5 Hz frequency before the least-squares method was used to fit an exponential function, $[R]_t = [R]_0 \times \exp(-k't)$, to the data. Here $[R]_t$ is the signal proportional to the radical concentration at time t, and k' is the pseudo-first-order rate constant under each experimental condition.

The CH_3/CD_3 radicals were generated from acetone/acetone-d_6:

$$CH_3C(O)CH_3/CD_3C(O)CD_3 + h\nu(193\ nm) \rightarrow 2CH_3/CD_3 + CO \quad (3a)$$

$$\rightarrow \text{other products} \quad (3b)$$

Lightfoot et al.[15] have shown that under conditions similar to these employed in this work, the photodissociaton of acetone proceed predominantly (>95%) via channel (3a). In addition, CH_3 radicals were produced from nitromethane[16]

$$CH_3NO_2 + h\nu(193\ nm) \rightarrow CH_3 + NO_2 \quad (4a)$$

$$\rightarrow \text{other products} \quad (4b)$$

or from 2,4-hexadiene:

$$CH_3CH{=}CHCH{=}CHCH_3 + h\nu(193\ nm) \rightarrow CH_3 + \text{other products} \quad (5a)$$

$$\rightarrow \text{other products} \quad (5b)$$

No information on the CH_3 radical quantum yields in the 193 nm photolysis of CH_3NO_2 or 2,4-hexadiene is available. These precursors, in addition to acetone, were used to confirm that the measured bimolecular reaction rate constants were independent of the identity of the methyl radical precursor employed.

The experiments were conducted under conditions where only two significant reactions consumed R ($R = CH_3$, CD_3):

$$R + Cl_2 \rightarrow \text{products} \quad (A)$$

$$R \rightarrow \text{heterogeneous and homogeneous loss} \quad (B)$$

The first-order decay rate constant of reaction B, denoted k_0, is a lump-sum of all first-order processes occurring in the reaction mixture and on the reactor wall without the added molecular reactant. The main contribution to k_0 is the heterogeneous loss of free radicals on the reactor wall. It was measured by reducing the precursor concentration and/or the laser intensity, that is by reducing the initial concentrations of free radicals, until the radical decay rate constant no longer depended on these factors and the exponential fit to the temporal ion signal showed no deviation from the first order decay. When these conditions were achieved, it was presumed that all radical−radical processes were suppressed (i.e., had negligible rates compared to the first-order processes occurring in the system). Initial methyl radical concentrations were then typically in the range $0.7-3.0 \times 10^{11}$ molecule cm^{-3}, which was estimated either from the laser fluencies and known absorption cross-sections of the precursors[17,18] at the wavelengths used or from the measured decompositions of the precursors.

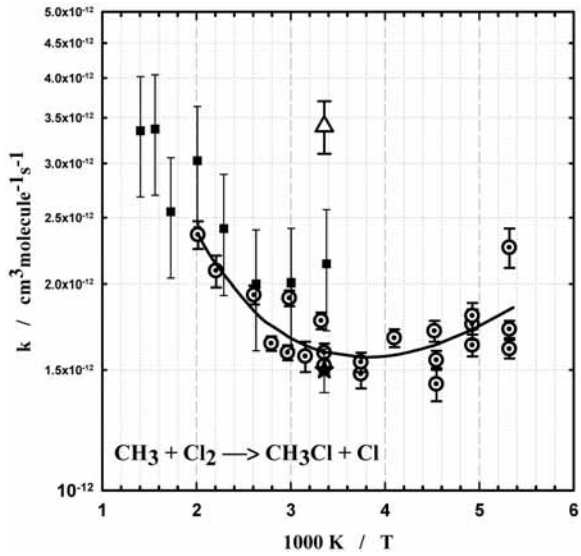

Figure 2. Semilog plot of the bimolecular rate constants for CH_3 + Cl_2 reaction versus 1000 K/*T*. Dotted circles: this work. Filled squares: Timonen and Gutman, 1986.[50] Star: Kovalenko and Leone, 1984.[49] Open triangle: Dobis and Benson, 2001.[51] Solid line: fit by modified Arrhenius expression, E1a (see text).

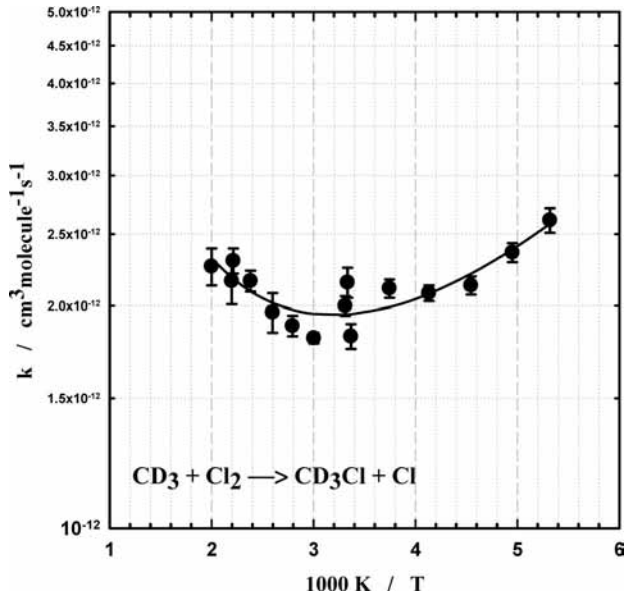

Figure 3. Semilog plot of the bimolecular rate constants for CD_3 + Cl_2 reaction versus 1000 K/*T*. Solid line: fit by modified Arrhenius expression (eq E1b).

The pseudo-first-order rate constant (k') was measured as a function of the Cl_2 concentration ($[Cl_2]$), which was always much higher (>20 times) than [R], resulting in pseudo-first-order reaction kinetics. Since the only significant processes consuming R during these experiments were the reaction with Cl_2 (A) and disappearance in the mainly heterogeneous reaction (B), the bimolecular reaction rate constant $k(R + Cl_2)$ could be obtained from the slope of the k' vs $[Cl_2]$ plot. The decay rate constants k' at the highest concentrations of Cl_2 were typically 10−30 times larger than k_0; therefore, the impact of small errors in k_0 on the reaction rate constant $k(R + Cl_2)$ was negligible. Values of k' were always determined from the concentration profiles of CH_3/CD_3 radical signal decays. A typical plot is shown in Figure 1 for the CH_3 + Cl_2 reaction at 188 K. Examples for CH_3 radical signal decay and CH_3Cl product formation profiles are also shown in Figure 1.

Radical precursors, $CH_3C(O)CH_3$ (Aldrich, purity ≥99.5%), $CD_3C(O)CD_3$ (Aldrich, purity ≥99.5%), CH_3NO_2 (Aldrich, purity ≥96%), and 2,4-hexadiene (Aldrich, purity >90%) were degassed before use. Helium (Messer-Griesheim purity of 99.9996%) and chlorine (Messer-Griesheim purity of 99.8%) were used as supplied without further purification.

Theoretical Calculations of the Potential Energy Surface for Reactions 1 and 2. There have been many prior computational investigations of the reaction CH_3 + HCl (reaction 1), or equivalently the reverse process, Cl + CH_4, but fewer analyses of reaction CH_3 + Cl_2 (reaction 2). These studies indicate the likely existence of bound intermediates along the reaction paths and, in the case of reaction 2, raise the question of whether the energy of the transition state (TS) is above or below that of the reactants. These issues can invalidate simple transition state theory (TST) analysis[11] and may complicate assessment of the role of quantum mechanical tunneling.

Reaction 1 plays a significant role as a test case for theoretical analysis. The earliest computational study of reaction 1 in 1989 by Truong et al. applied MP2 and MP4 second-order and fourth-order perturbation theory together with an empirical scaling of correlation corrections (SAC) to quantify the barrier for this reaction.[19] The study of Chen et al. was based on Gaussian-1 theory and drew attention to possible bound intermediates in the entrance and exit channels.[20] They derived rate constants via RRKM theory with a simple Wigner tunneling correction. In 1994 Dobbs and Dixon applied MP2 theory and density functional theory (DFT) to the geometries of the reactants, products, and TS, followed by single-point quadratically converged configuration interaction and coupled cluster calculations with single, double, and perturbative triple excitations, QCISD(T) and CCSD(T), respectively.[21] Rate constants were derived via canonical transition state theory (TST) combined with a Wigner tunneling model. Duncan and Truong applied MP4 theory with DFT geometries and frequencies to derive rate constants via canonical variational TST (CVTST) and included a small-curvature tunneling (SCT) correction.[22] Espinosa-Garcia and Corchado constructed a potential energy surface (PES) from MP2/SAC data and derived rate constants and kinetic isotope effects (KIEs) via CVTST combined with a large-curvature tunneling model.[23] Espinosa-Garcia and co-workers have continued this theme with two further studies based on refined PESs derived from CCSD(T) results at the double and triple-ζ extrapolated to the infinite basis limit and from Gaussian-3 data, respectively.[24,25] Their 2000 PES was also employed by Martinez-Nunez et al. in a semiclassical trajectory analysis.[26] In 1999 Yu and Nyman conducted quantum scattering calculations, which inherently incorporate tunneling, based on their MP2/SAC PES.[27] Two experimental studies employed MP2 data and one-dimensional Eckart tunneling to rationalize rate constants for Cl with CH_4 and deuterated methanes.[28,29] Hartree−Fock and MP2 calculations were used in a demonstration of on-the-fly classical trajectories.[30] Troya et al. applied MP4 theory to points along the reaction coordinate for CVTST analysis and fitted their data to a new PES for quasiclassical trajectory (QCT) analysis.[31] Reaction 1 continues to be a focus of theoretical attention, and the past year has seen development of a new PES,[32] a VTST study,[33] two QCT studies,[34,35] and a quantum scattering analysis.[36]

Tirtowidjojo et al. used Gaussian-2 theory to investigate reaction 2.[37] Use of MP2/6−31G(d) geometries and HF/6−31G(d) frequencies led to a computed barrier of −1.6 kJ mol^{-1} relative to reactants, which increased to +16.3 kJ mol^{-1} when QCISD/6−311G(d,p) values for these quantities were

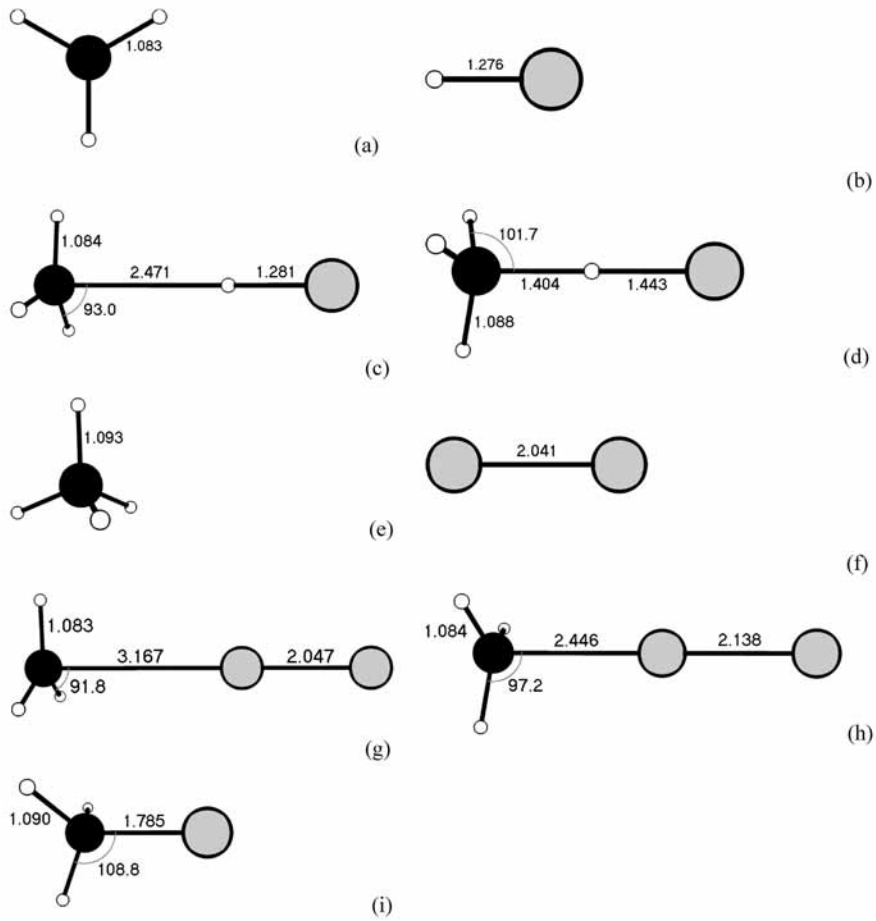

Figure 4. QCISD/6−311G(d,p) structures, with distances in angstroms and angles in degrees. (a) D_{3h} CH_3; (b) HCl; (c) C_{3V} CH_3−HCl complex; (d) C_{3V} CH_3−HCl transition state; (e) T_d CH_4; (f) Cl_2; (g) C_{3V} CH_3−Cl_2 complex; (h) C_{3V} CH_3−Cl_2 transition state; (i) C_{3V} CH_3Cl.

employed. They did not calculate rate constants but compared experimental values with their ab initio pre-exponential factor to derive a fitted barrier of +0.8 kJ mol^{-1}. Seetula applied MP2/6−31G(d,p) theory to the TS and obtained an entropy of activation 25 J K^{-1} mol^{-1} lower than experiment at 298 K, which corresponds to an underestimation of the pre-exponential factor by a factor of 20.[9] Lee et al. applied CBSQ theory at MP2/6−311G(d,p) geometries to characterize a CH_3−Cl_2 adduct bound by 6.1 kJ mol^{-1}, followed by a TS below this in energy. The computed enthalpy of activation at 298 K was −11.4 kJ mol^{-1} and was corrected upward by 9.6 kJ mol^{-1} for improved agreement between TST and experiment.[38] Drougas et al. used the 6−311+G(3df,2p) basis set and applied CCSD(T) theory at MP2 geometries to derive a reaction barrier of 5.2 kJ mol^{-1} and characterized complexes between the reactants and between the products, bound by 3.6 and 9.3 kJ mol^{-1}.[39] They argued that the former complex could be neglected and analyzed the kinetics via RRKM modeling of decomposition of the CH_3Cl−Cl complex and via quasiclassical trajectories on a LEPS surface constructed to include this complex and the TS.

To summarize, the kinetics of reaction 1 may be well-reproduced by sophisticated calculations such as quantum scattering and variational TST, which require extensive information about the PES. The kinetics of reaction 2 have not been studied to the same extent and have yet to be rationalized quantitatively. Here we explore a methodology that could be readily extended to larger systems, because it is focused on stationary points on the PES. The calculations here use CCSD(T) theory for high accuracy, with basis sets extrapolated to the infinite limit. At this limit any basis set superposition error (BSSE) is eliminated. The energies of stationary points for reaction 2 should be more accurate than previous ones and in particular enable definitive assessment of a bound complex and a negative TS energy.

Methodology for Calculations. Stationary points and the reaction path were investigated using spin-unrestricted QCISD theory with the 6−311G(d,p) atomic basis set. The reactants, loosely bound complexes, and TSs between these species and the final products CH_4 + Cl (reaction 1) and CH_3Cl + Cl (reaction 2) were characterized, and their geometries and frequencies are summarized in Figure 4 and Tables 2 and 3. These calculations were carried out with the Gaussian 03 program suite.[40] The ab initio frequencies have been scaled by a standard factor of 0.954,[41] to account for anharmonicity. This factor is very close to the value of 0.955 derived previously for a variety of halomethanes and halocarbon radicals.[42,43] The intrinsic reaction coordinate was explored in the neighborhood of the TS, and projected vibrational frequencies were scaled in the same way to obtain the vibrational zero-point energy (ZPE) near the saddle point.

Next, high accuracy energies were obtained at points along the QCISD/6−311G(d,p) reaction coordinate via coupled cluster theory. The Molpro 2002.6 program[44] was used to compute spin-unrestricted CCSD(T) energies with correlation consistent basis sets, based on spin-restricted Hartree−Fock wave functions. The aug-cc-pVnZ basis sets of Peterson et al.[45] with n from 2 to 4 were employed for reaction 1, and the analogous aug-cc-pV(n+d)Z basis sets for reaction 2.[46] Results for the stationary points are included in Tables 2 and 3. The energy at the infinite

TABLE 1: Results and Conditions of the Experiments[a] Used To Measure the Bimolecular Rate Constants of the Reaction R + Cl_2 → products (R = CH_3 and CD_3)

T/K	p/Torr[b]	$[Cl_2]/10^{13}$ molecule cm^{-3}	k_0/s^{-1}[c]	$k/10^{-12}$ cm^3 molecule^{-1} s^{-1}[d]
		$CH_3 + Cl_2 \rightarrow CH_3Cl + Cl$		
188[e]	1.0	0.6−10.0	16	1.72 ± 0.05
188	1.0[f]	1.6−8.7	12	1.61 ± 0.05
188	2.0	0.7−9.8	14	2.26 ± 0.15
203[e]	1.1[g]	1.3−11.4	18	1.63 ± 0.06
203	1.0	2.6−7.4	13	1.75 ± 0.09
203	2.1	2.2−14.1	12	1.80 ± 0.08
220[e]	1.0	0.6−9.4	19	1.55 ± 0.05
220	1.1	2.3−11.9	13	1.43 ± 0.08
221[h]	1.0	1.0−8.6	5	1.71 ± 0.06
244	1.0	1.9−16.9	15	1.67 ± 0.05
267	1.0	2.1−15.3	15	1.48 ± 0.07
267[e]	1.0	1.9−10.7	11	1.54 ± 0.05
298[h]	1.0	1.6−8.0	6	1.59 ± 0.05
298	0.6[i]	1.0−7.3	12	1.52 ± 0.03
301	5.1	1.6−11.4	10[j]	1.77 ± 0.05
317[e]	1.0[g]	0.9−10.5	14	1.57 ± 0.08
335	2.9	2.4−12.8	9[j]	1.91 ± 0.05
337[e]	1.0	1.4−11.0	11	1.59 ± 0.04
358	1.0	0.9−13.1	5	1.64 ± 0.04
383	5.4	1.6−13.1	11[j]	1.93 ± 0.06
453	7.7	2.5−14.3	14[j]	2.09 ± 0.11
496	6.0	2.0−9.5	25[j]	2.36 ± 0.11
		$CD_3 + Cl_2 \rightarrow CD_3Cl + Cl$		
188	1.0	0.7−10.4	11	2.61 ± 0.10
202	1.0	0.5−9.9	10	2.36 ± 0.07
220	1.0	0.9−8.8	10	2.13 ± 0.06
242	1.0	1.9−8.3	7	2.08 ± 0.05
267	1.1	1.5−10.7	6	2.11 ± 0.06
297	1.1	1.0−10.9	11	1.82 ± 0.07
300	5.1	1.9−11.7	9[j]	2.15 ± 0.10
302	5.1	3.6−14.5	10[j]	2.00 ± 0.06
333	1.1	0.9−10.6	7	1.81 ± 0.03
358	1.0	1.0−11.0	11	1.88 ± 0.06
385	6.6	1.8−16.8	14[j]	1.96 ± 0.12
420	6.9	2.0−12.5	14[j]	2.16 ± 0.07
452	7.6	4.1−12.0	21[j]	2.30 ± 0.09
455	7.6	4.3−15.7	19[j]	2.16 ± 0.15
500	8.1	1.8−11.1	37[j]	2.26 ± 0.13

[a] CH_3COCH_3 and CD_3COCD_3 used as precursors for CH_3 and CD_3 radicals employing 193 nm radiation unless otherwise stated. Range of precursor concentrations used: (3.5−8.8) × 10^{12} molecule cm^{-3} for CH_3COCH_3, (0.9−3.0) × 10^{12} molecule cm^{-3} for CH_3NO_2, and (1.7−17.4) × 10^{12} molecule cm^{-3} for CD_3COCD_3. Estimated initial radical concentrations employed (0.7−3.0) × 10^{11} molecule cm^{-3}. [b] Helium used as a buffer gas. [c] Pyrex-glass reactor tube with 17 mm inner diameter (i.d.) coated with halocarbon wax used unless otherwise stated. [d] Statistical uncertainties shown are 1σ; estimated overall uncertainty is ±20%. [e] CH_3NO_2 (193 nm) used as a precursor. [f] A few decay rates measured at 0.5 torr and 2 torr pressure; no dependence on pressure was observed. [g] A few decay rates measured at about three times higher buffer gas pressure (3 torr); no dependence on pressure was observed. [h] 2,4-Hexadiene (193 nm) used as a precursor. [i] A few decay rates measured at about five times higher buffer gas pressure (5 torr); no dependence on pressure was observed. [j] Stainless steel reactor tube with 8 mm i.d.

n or complete basis set limit, E_{CBS}, was obtained via extrapolation of these data as a function of n:[47]

$$E_n = E_{CBS} + A \exp(-Bn)$$

Addition of the isotope-dependent ZPE yielded the vibrationally adiabatic ground-state (VAG) potential energy surface, including the barrier height and reaction enthalpy. These results are plotted in Figures 5 and 6 where again an empirical

TABLE 2: Ab Initio Energies and Frequencies for Stationary Points on the CH_3 + HCl Potential Energy Surface[a]

species	QCISD/6−311G(d,p) energy, au	frequencies scaled by 0.955 with degeneracies, cm^{-1}	CCSD(T) energy, au				relative classical energy,[b] kJ mol^{-1}	relative enthalpy at 0 K,[b] kJ mol^{-1}
			aug-cc-pVDZ	aug-cc-pVTZ	aug-cc-pVQZ	CBS		
CH_3	−39.72916	413, 1370 (2), 2984, 3157 (2)	−39.72449	−39.76362	−39.77327	−39.77644	0	0
HCl	−460.26031	2905	−460.27215	−460.34324	−460.36417	−460.37290		
adduct	−499.99231	75, 105 (2), 254 (2), 534, 1371 (2), 2845, 2978, 3151 (2)	−500.00063	−500.11054	−500.14097	−500.15261	−8.6	−3.6
TS	−499.98281	1175i, 340 (2), 482, 896 (2), 1152, 1382 (2), 2957, 3108 (2)	−499.99483	−500.10472	−500.13492	−500.14637	7.8	11.9
CH_4	−40.40164	1304 (3), 1501 (2), 2906, 3020 (3)	−40.39560	−40.44090	−40.45167	−40.45502	−24.3	−3.2
Cl	−459.60167	-	−459.61219	−459.67619	−459.69471	−459.70224		

[a] 1 au = 2625.5 kJ mol^{-1}. [b] Includes −3.5 kJ mol^{-1} spin−orbit correction for atomic Cl.

TABLE 3: Ab Initio Energies and Frequencies For Stationary Points on the $CH_3 + Cl_2$ Potential Energy Surface[a]

species	QCISD/6−311G(d,p) energy, au	frequencies scaled by 0.955 with degeneracies, cm^{-1}	CCSD(T) energy, au				relative classical energy,[b] kJ mol^{-1}	relative enthalpy at 0 K,[b] kJ mol^{-1}
			aug-cc-pVDZ+d	aug-cc-pVTZ+d	aug-cc-pVQZ+d	CBS		
CH_3	−39.72916	413, 1370 (2), 2984, 3157 (2)	−39.72449	−39.76362	−39.77327	−39.77644	0	0
Cl_2	−919.26253	498	−919.30981	−919.44254	−919.48267	−919.50006		
adduct	−958.99372	40 (2), 68, 127 (2), 480, 494, 1370 (2), 2981, 3156 (2)	−959.03771	−959.20926	−959.25896	−959.27924	−7.2	−4.5
TS	−958.99029	330i, 61 (2), 315, 438 (2), 845, 1373 (2), 2979, 3149 (2)	−959.03767	−959.20891	−959.25831	−959.27834	−4.9	2.5
CH_3Cl	−499.45585	730, 1011 (2), 1372, 1427 (2), 2955, 3049 (2)	−499.47175	−499.57783	−499.60800	−499.62000	−127.2	−108.8
Cl	−459.60167	-	−459.61804	−459.67783	−459.69585	−459.70363		

[a] 1 au = 2625.5 kJ mol^{-1}. [b] Includes −3.5 kJ mol^{-1} spin−orbit correction for atomic Cl.

Figure 5. Sketch of the vibrationally adiabatic potential energy diagram for $CH_3 + HCl \rightarrow CH_4 + Cl$.

spin−orbit correction has been included in the atomic Cl energy. In these plots, adducts between the products have been neglected.

The imaginary vibrational frequency at the TS, which corresponds to displacement along the reaction coordinate, is important for assessing the width of the barrier and the extent of quantum mechanical tunneling. Two approaches were tried in the present work. First, the frequency was obtained at the QCISD/6−311G(d,p) level, which corresponds to the curvature in a classical (no ZPE) PES. A more realistic effective barrier is found on the VAG PES, because it incorporates changes in ZPE along the reaction coordinate, and the underlying classical energy is derived from infinite-basis-set CCSD(T) results. The region of the reaction coordinate close to the QCISD/6−311G(d,p) TS (changes in reaction coordinate up to ±0.2 $amu^{1/2}$ bohr) was explored in more detail: projected ZPEs and CCSD(T)/CBS energies were combined, and the maximum found by interpolation. The curvature of this VAG PES was assessed in an approximate manner. The reacting system was treated as an effectively three-particle linear system ABC, with A = CH_3, B = H or Cl, and C = Cl. Within the central force approximation the energy changes in a small region close to the saddle point of the VAG PES can be written as $1/2(k_1x_1^2 + k_2x_2^2)$, where x_1 is the extension of the A−B bond from the saddle-point value, x_2 is the extension of the B−C bond from its value at the saddle point, and k_1 and k_2 are the stretching force constants. The latter two quantities were obtained for each isotope combination by fitting computed VAG PES points close to the saddle point, where changes in the bond lengths were up to about 0.15 Å. Solving for the two stretching frequencies via the relations given by Herzberg (see page 173 in ref 48) yields the imaginary mode for the linear ABC system. Development of the VAG PES and solution for the imaginary frequency was repeated for each isotope combination, and the results are listed in Table 4, along with the barrier heights adjusted for changes in ZPE.

Results and Discussion

Experimental Results. The measured bimolecular rate constants for the $CH_3 + Cl_2$ and $CD_3 + Cl_2$ reactions are given in Table 1 together with their statistical uncertainties (±1σ) and the experimental conditions. The estimated overall uncertainties of the measured rate constants are about ±20%. These arise mainly from the uncertainties in the determining the reactant concentrations and from the uncertainties in the pseudo first-order rate constants. Semilogarithm plots of the bimolecular rate

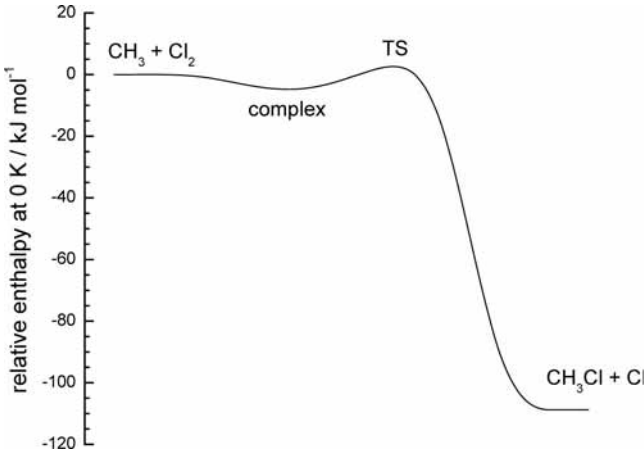

Figure 6. Sketch of the vibrationally adiabatic potential energy diagram for $CH_3 + Cl_2 \rightarrow CH_3Cl + Cl$.

constants for the $CH_3 + Cl_2$ and $CD_3 + Cl_2$ reactions versus 1000 K/*T* (Arrhenius coordinates) are shown in Figures 2 and 3. The rate constant for the $CH_3 + Cl_2$ reaction (reaction 2a) was previously directly measured by Kovalenko and Leone at ambient temperature using time-resolved IR luminescence,[49] by Timonen and Gutman over the temperature range 298−712 K using a flow reactor coupled to a photoionization mass spectrometer,[50] and by Dobis and Benson at ambient temperature using very low pressure reactor (VLPR) technique.[51] The results of these measurements are shown in Figure 2 together with the results of the current work. Current measurements are in excellent agreement with the single temperature measurement of Kovalenko and Leone and agree within the experimental error with the earlier measurements of Timonen and Gutman. However, the bimolecular reaction rate constant derived by Dobis and Benson employing the VLPR technique for the $CH_3 + Cl_2$ reaction at ambient temperature is about factor of 3 larger than that obtained in this work and in the other previous determinations. On the other hand, for the $C_2H_5 + Cl_2$ reaction, an even more pronounced difference exists between the results of Eskola, Lozovsky et al.[52] which are in good agreement with previous determinations[50] and that obtained by Dobis and Benson. Their bimolecular rate constant at 298 K for the ethyl + Cl_2 reaction is lower than the other values by a factor of 10 or more. In the pioneering experimental work on the methyl radical reactions with Br_2, Cl_2, and BrCl, Evans and Whittle[53] measured the kinetics of $CH_3 + Cl_2$ relative to the $CH_3 + Br_2$ reaction as a function of temperature between 321 and 472 K. For the ratio $k(CH_3 + Cl_2)/k(CH_3 + Br_2)$ they obtained 0.0359 and 0.0881 at temperatures 325 and 450 K, respectively. Combination of current results with the available data for the $CH_3 + Br_2$ reaction at these temperatures[54] results in the ratios of 0.048 and 0.067 at temperatures 325 and 450 K. Some differences exist between $k(CH_3 + Cl_2)/k(CH_3 + Br_2)$ ratios obtained by Evans and Whittle and the ratios calculated from the results of this work ($CH_3 + Cl_2$ reaction) and from the work of Timonen, Seetula et al. ($CH_3 + Br_2$ reaction), in particular in the magnitude of the positive temperature dependence of this ratio. However, on average the agreement is good and there is consistency between these studies.

All previous measurements were performed at ambient and elevated temperatures and yielded positive temperature dependences (positive apparent activation energies). In the current work, the measurements were extended down to temperatures as low as 188 K. The data show the change of the sign of the temperature dependences at about 270−300 K and negative temperature dependence (negative apparent activation energy) at lower temperatures. The apparent activation energy for the $CH_3 + Cl_2$ reaction is about 2.6 kJ/mol above ca. 270 K and changes to about −0.9 kJ/mol at temperatures below ca. 270 K.

Reaction of D-substituted methyl radical, $CD_3 + Cl_2$ (Reaction 2b) is faster than reaction 2a, $CH_3 + Cl_2$. Deuterium substitution increases the rate constant, in particular at low temperatures, where the effect reaches ca. 45% at 188 K. The measurements also indicate the change of the sign of the temperature dependence at about 300 K (Figure 3). There have been no prior measurements of the kinetics of this reaction. For the $CD_3 + Cl_2$ reaction the apparent activation energy above ca. 300 K is about 1.7 kJ/mol, which changes to about −1.3 kJ/mol at temperatures below 300 K.

The experimental rate constants of the $CH_3 + Cl_2$ as well as $CD_3 + Cl_2$ reactions are lower than the rate constants of the reactions of larger hydrocarbon radicals in similar reactions under the same conditions[50,52] but larger than the rate constants of halogenated methyl radicals.[5,55] The temperature dependences of these rate constants in Arrhenius coordinates ($\ln(k)$ vs $1/T$) are linear at temperatures 298−498 K and slightly negative for the larger hydrocarbon radicals (except for *tert*-butyl radical where there is no dependence), slightly positive for methyl (2.2 kJ/mol), and positive for the halogenated methyl radicals (8−22 kJ/mol).[5,50,55] A similar negative temperature dependence as mentioned above was measured by Eskola, Lozovsky et al. for some larger hydrocarbon radicals (ethyl, *n*-propyl, *n*-butyl) also at lower temperatures (200−298 K).[52]

The rate constants for reactions $2_{a,b}$ obtained in this work were fitted by the modified Arrhenius expression over the experimental temperature range:

$$k_{2a} = 1.7 \times 10^{-13} (T/300\ \mathrm{K})^{2.52} \exp(5520\ \mathrm{J\ mol^{-1}}/\mathrm{RT})\ \mathrm{cm^3\ molecule^{-1}\ s^{-1}} \quad \text{(E1a)}$$

$$k_{2b} = 2.9 \times 10^{-13} (T/300\ \mathrm{K})^{1.84} \exp(4770\ \mathrm{J\ mol^{-1}}/\mathrm{RT})\ \mathrm{cm^3\ molecule^{-1}\ s^{-1}} \quad \text{(E1b)}$$

The solid lines in figures 2 and 3 correspond to equations E1a,E1b.

Results of Calculations. The overall computed reaction enthalpy for reaction 1, combined with an empirical spin−orbit correction for atomic Cl, is −3.2 kJ mol^{-1} This is in good accord with the experimental value of −5.07 ± 0.14 kJ mol^{-1}, equal to the difference between the CH_4 and HCl bond dissociation enthalpies at 0 K taken from the IUPAC recommendation[56] and the Active Thermochemical Tables.[57] Any errors in the computed bond strengths are therefore well-balanced and appear to cancel along the reaction coordinate. Much of the discrepancy in $\Delta_r H^0_0$ arises from the ZPE of the out-of-plane vibrational mode of CH_3, where severe anharmonicity leads to a frequency about 200 cm^{-1} higher than computed. If this is corrected, the computed $\Delta_r H^0_0$ becomes 1.2 kJ mol^{-1} more negative, i.e., closer to experiment.

The TS is computed to lie 11.9 kJ mol^{-1} above CH_3 + HCl. Essentially the same value, 11.7 kJ mol^{-1}, was derived by Troya and Weiss who applied similar energy calculations to those performed here, combined with CCSD(T)/aug-cc-pVTZ geometries and frequencies.[34] Comparison with the VAG PES results indicates that location of the TS at the QCISD saddle-point geometry, rather than the local VAG PES maximum, introduces a negligible error of less than 0.1 kJ mol^{-1} in the barrier. There is also only a minor difference in geometry, with the VAG

TABLE 4: Computed Barrier Heights and Imaginary Frequencies for the Vibrationally Adiabatic CCSD(T)/CBS Potential

reaction	calculated forward barrier, kJ mol^{-1}	imaginary harmonic frequency, cm^{-1}	imaginary vibrationally adiabatic frequency, cm^{-1}	barrier used in calculations, kJ mol^{-1}
$CH_3 + HCl \rightarrow CH_4 + Cl$	11.9	1175i	1362i	11.9
$CH_3 + DCl \rightarrow CH_3D + Cl$	14.1	892i	814i	14.1
$CD_3 + HCl \rightarrow CHD_3 + Cl$	9.3	1163i	1464i	9.3
$CD_3 + DCl \rightarrow CD_4 + Cl$	11.5	886i	849i	11.5
$CH_3 + Cl_2 \rightarrow CH_3Cl + Cl$	2.5	330i	474i	1.6
$CD_3 + Cl_2 \rightarrow CD_3Cl + Cl$	0.3	326i	553i	−0.6

results for the C−H and H−Cl distances in the TS greater and smaller than the QCISD data (Figure 4) by about 0.015 Å. The curvature of the VAG PES is however significantly smaller than in the classical QCISD PES, as reflected in the smaller imaginary frequencies (Table 4).

The TS in reaction 1 is preceded by a complex, thought to be bound by interaction between the HCl dipole and the CH_3 quadrupole.[31] The strength of this interaction is not known experimentally. Our computed binding energy of 3.6 kJ mol^{-1} is slightly greater than the original G1 result of Chen et al.,[20] 2.6 kJ mol^{-1}, but smaller than the value of 8.0 kJ mol^{-1} derived by Troya and Weiss.[34]

The enthalpy of reaction 2 is more challenging computationally. We obtain −108.8 kJ mol^{-1}, in reasonable accord with the experimental value of −104.3 ± 0.6 kJ mol^{-1} at 0 K, based on the heats of formation of CH_3,[56] Cl,[57] and CH_3Cl.[41] Extrapolation of basis sets without tight polarization functions yielded a slightly worse result of −110.3 kJ mol^{-1}. Consideration of the CH_3Cl and Cl_2 bond strengths indicates that our best calculations accurately describe the C−Cl bonding (underestimated by 1.0 kJ mol^{-1}, an error which is comparable to the experimental uncertainty[41] of 0.6 kJ mol^{-1}), but that Cl−Cl binding is underestimated by 5.5 kJ mol^{-1}. Our result is an improvement over prior calculations. The initial study by Tirtowidjojo et al.[37] employed G2 and related methods; the G2 value of $\Delta_r H_0$ is −113.4 kJ mol^{-1}. The CBSQ calculations of Lee et al. and CCSD(T)//MP2/ 6−311+G(3df,2p) calculations of Drougas et al. yielded $\Delta_r H_0$ values of −135.9 and −126.4 kJ mol^{-1}, respectively. These three results would become 3.5 kJ mol^{-1} more negative, i.e., further from experiment, if spin−orbit coupling in Cl were taken into account.

Similarly to reaction 1, comparison of the classical QCISD and interpolated VAG saddle points indicates the C−Cl distance in the QCISD TS is about 0.04 Å too large and the Cl−Cl separation is 0.02 Å too small. Neglect of the high level interpolation causes an error in the barrier of 0.1 kJ mol^{-1}.

Theoretical Calculations of the Rate Constants for Reactions 1 and 2. The calculations of the rate constants for reactions 1 and 2 were performed based on the transition state theory with 1D tunneling correction. In reaction 2, a slight correction of the TS energy brings this energy to negative values; therefore, the modified transition state theory was used.[11,13]

Reaction $CH_3(CD_3)$ + HCl(DCl) (reaction 1). In reactions 1a−d, the calculated barriers are relatively large (9 to 14 kJ mol^{-1}) and are *positive* beyond any uncertainties of the calculations. The only reason for the strongly curved Arrhenius plots in this case is quantum tunneling, whose role increases at low temperatures. At the highest temperatures of the experiment (ca. 500 K), tunneling corrections are relatively small (about a factor of 1.6−1.5 for reactions 1a,b and a factor of 1.33 for reactions 1c,d) and are almost the same irrespective of the 1D tunneling model used. However, since the estimated quantum corrections at low temperatures are large (up to 1 order of magnitude for reactions 1a−d at ca. 200 K), usual first-order corrections (such as the Wigner tunneling correction[58] and similar corrections) are not applicable. Moreover, the expression for tunneling through the infinite parabolic potential,[59,60] used in the original version of the modified transition state theory[11] to calculate small tunneling corrections, is not applicable at low temperatures due to divergence. To avoid this divergence, finite potentials, such as the truncated parabolic[61,62] and the Eckart potential,[63,64] were used to calculate the tunneling factors in reactions 1 and 2.

There are several uncertain issues that should be clarified when using finite height potentials, such as the truncated parabola and the Eckart potential, to calculate 1D tunneling corrections. One such issue is the imaginary frequency of the transition state, which is used to approximate the widths of such barriers. This frequency depends upon the choice of the 1D potential along the reaction coordinate. The two extremes are (i) choosing the profile of the electronically adiabatic PES and assuming complete decoupling of the vibrational modes of the "transition state" from the motion along the reaction coordinate, and (ii) assuming that all vibrational modes of the TS are "fast degrees of freedom" compared to the motion along the reaction coordinate, and constructing the "vibrationally adiabatic" PES. The latter case is analogous to the Born−Oppenheimer approximation for the separation of the motion of nuclei from electronic motion in molecules. In this case, the zero-point energy of the vibrational modes of the TS is added to the electronically adiabatic PES.

One can argue that for reaction 1, where the imaginary TS frequency is relatively large compared to the frequencies of the "transitional modes" of the TS (i.e., the vibrational modes that do not exist in the reactants and the modes whose frequency undergoes significant changes in the course of reaction), the first approximation seems to be more reasonable. It means that for reaction 1 and the isotope analogues, better results are expected when usual harmonic frequencies calculated on the electronically adiabatic PES are used for the tunneling calculations. However, in reaction 2, with a relatively low harmonic imaginary frequency, almost all the transitional modes are of higher frequency, and therefore, are "fast" degrees of freedom. The only low frequency bending mode of the TS (ca. 60 cm^{-1}) provides only a minor contribution to zero-point energy. Therefore, using the "vibrationally adiabatic PES", that is, the electronically adiabatic PES plus the zero-point vibrational energy for the calculation of the imaginary frequency of the TS, is considered to be a more realistic approximation in this case.

The second issue that should be addressed is related to the presence of the shallow wells at the entrance and the exit of the reactant and product valleys. The extreme choices here are the calculation of the barrier height from the bottoms of these wells, which results in the highest barrier, or using the cross-section of the PES obtained by linear extension of the reaction

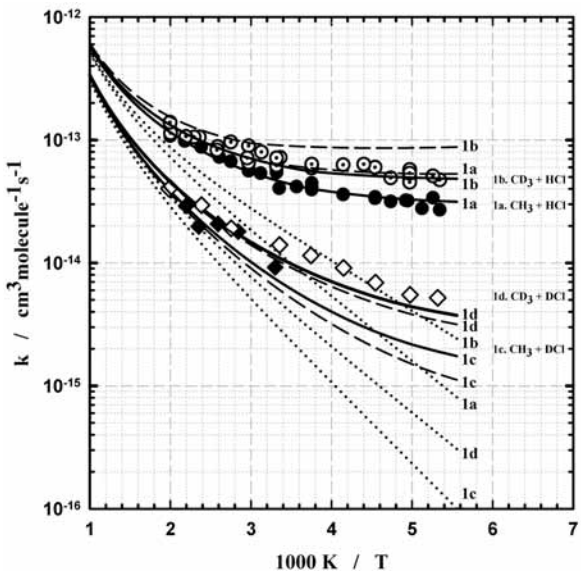

Figure 7. Rate constants for reactions 1a−d. Symbols: experiment.[12] Solid circles, open circles, solid diamonds, open diamonds for reactions 1a (CH_3 + HCl), 1b (CD_3 + HCl), 1c (CH_3 + DCl), and 1d (CD_3 + DCl), respectively. Lines: current calculations. Dotted lines: transition state theory (TST) without tunneling. Solid lines: TST with 1D tunneling through a truncated parabolic barrier, harmonic frequencies. Dashed line: TST with 1D tunneling through a truncated parabolic barrier, vibrationally adiabatic frequencies. Parameters: see Table 4.

normal mode beyond the quadratic potential,[64] resulting in the smallest barrier height. In 1D tunneling calculations this issue is usually ignored, and the barrier height is usually taken relative to the ground-state of the reactants. Such a choice justifies the truncated parabola as a better representation of the potential (compared to the Eckart potential) for tunneling calculations. Too rigorous a consideration of these issues is, probably, not justified in view of known limitations of the 1D tunneling approach due to the multidimensional "corner cutting" effect (e.g., ref 65 and references therein).

In the current calculations, we used an infinite parabolic barrier (for relatively high temperatures), a truncated parabolic potential, and a (symmetric) Eckart potential. We report the results obtained with the truncated parabolic potential and note that the calculations with the symmetric Eckart potential yielded similar results (after some adjustment of the imaginary frequencies).

The results of the calculations are shown in Figure 7. Dotted lines represent calculations using TST without tunneling, and the solid lines are the results obtained by the TST and 1D tunneling corrections with the truncated parabolic potential based on the harmonic imaginary frequencies of the transition states listed in Table 4. The dashed lines were calculated using the vibrationally adiabatic imaginary frequencies. No adjusted parameters were used in these calculations. The agreement between the calculations with the harmonic frequencies and the experiment at 500 K is very good; the maximum deviation is +14% for reaction 1d, within the experimental error. The average k_{calc}/k_{exp} at 500 K for all four isotopomer reactions 1a−d is 1.01. Moreover, the calculations reproduce both the shape of the curves as well as the absolute values of the rate constants over the whole temperature range, 185−500 K. The maximum deviation is ca. −25% observed at ca. 250 K for reaction 1d. Such a good agreement is of course fortuitous, in view of the sensitivity of the tunneling corrections to the imaginary frequencies of the TSs, to the tunneling model and to the limitations of the 1D models, as well as the accuracy of the theoretical calculations. However, the excellent agreement observed at high temperatures requires some comments. As was mentioned, the tunneling corrections at 500 K are relatively small and are expected to be calculated reasonably reliably. The results obtained with the infinite parabolic potential and the truncated parabolic potential are almost identical at these temperatures, which indicates that the tunneling occurs at the top of the barrier; presumably, multidimensional effects are not significant. Transition state theory provides an upper estimate for the rate constant. Theoretical calculations usually overestimate the barrier. These two factors impact the rate constant in the opposite directions, and, apparently, if present, they cancel out for reaction 1. Assuming that the transition state theory is accurate within a factor of 1.5−2, one can estimate the barrier accuracy in the current calculations as 1.7−3 kJ mol^{-1}.

In the previous publication[12] tunneling was dismissed based upon an overly simplified model of tunneling through a rectangular barrier and by the apparently successful rationalization of the primary and secondary kinetic isotope effects (KIE) with a classical approach. However, more realistic calculations performed in this work for tunneling either through a truncated parabolic or an Eckart barrier indicate that tunneling is important already when using 1D tunneling models. Moreover, estimates of the kinetic isotope substitution effects demonstrate that the KIE is much less sensitive a parameter to establish the role of tunneling by comparison with the absolute values of rate constants. For example, the experimental value of k_{1b}/k_{1d} is ca. 9.2 at 200 K. The calculated primary isotope substitution effect at 200 K is $k_{1b}/k_{1d} = 6.72$ without tunneling (−27% compared to the experimental value) and 11.29 with tunneling (+23%). Apparently, no conclusion on the role of tunneling can be reliably derived based just on the primary kinetic isotope substitution effect. For the secondary kinetic isotope substitution effect, k_{1a}/k_{1b}, the experimental value at 200 K is ca. 0.6. The calculated value is $k_{1a}/k_{1b} = 0.39$ (−35% compared to the experiment) without tunneling, and $k_{1a}/k_{1b} = 0.66$ (+10%) with tunneling. In this case the agreement with experiment when tunneling is taken into account is better. However, it is clear that the sensitivity of the KIE to tunneling is much less than the sensitivity of the absolute rate constants (such as a factor of 1.6 or so compared to a factor of 10 to 20).

Reaction $CH_3(CD_3)$ + Cl_2 (reaction 2). The results of the calculations together with the experimental data are shown in Figure 8. In the case of reaction 2, contrary to reaction 1, no agreement was achieved based on the results of the calculations without some adjustments. First, at 500 K, where the tunneling corrections are small (about 18% for both reactions 2a and 2b) and are determined reliably, the predicted rate constant with the calculated barrier of 2.5 kJ mol^{-1} (for reaction 2a) was ca. 24% smaller than the experimental rate constant. Therefore a small reduction of the barrier height by 0.9 kJ mol^{-1}, well within the ab initio uncertainty, was made to fit the rate constant of reaction 2a to the experimental data at high temperatures. Such a reduction brought the position of the barrier for reaction 2b to a negative value (−0.6 kJ mol^{-1}), and therefore the modified TST was used.[11,13] Second, it was found that neither the harmonic imaginary frequencies (330i and 326i cm^{-1}) nor even the vibrationally adiabatic (474i and 553i cm^{-1} for reactions 2a and 2b, respectively) were large enough to explain the shape of the temperature dependences of the experimental rate constants (Figure 8). Low imaginary frequencies indicate a wide barrier and, subsequently, low tunneling probability. To explain the shape of the curves in Figure 8 and the absolute values of

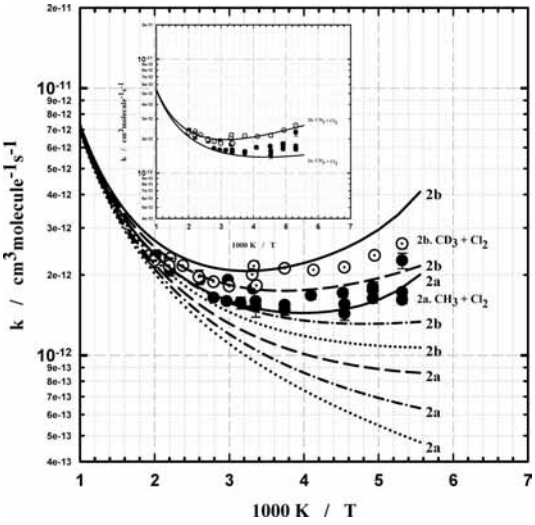

Figure 8. Rate constants for reactions 2a,b. Current work. Symbols, experiment; lines, calculations. Solid circles: reaction 2a ($CH_3 + Cl_2$). Open circles: reaction 2b ($CD_3 + Cl_2$). In all calculations the barrier was shifted down by 0.9 kJ mol^{-1}. Dotted lines: transition state theory without tunneling. Other lines: modified TST,[11] tunneling through an infinite parabolic potential. Dash-dotted line: harmonic imaginary frequencies. Dashed line: vibrationally adiabatic imaginary frequencies. Solid lines: the imaginary frequencies of the TSs are both set arbitrarily to 680 cm^{-1} (compared with the harmonic 330 and 326 and the vibrationally adiabatic, 474 and 553 cm^{-1}, for $CH_3 + Cl_2$ and $CD_3 + Cl_2$, respectively, see Table 4). Insert: the barrier heights reduced by 3 kJ mol^{-1}, harmonic frequencies, all rate constants multiplied by a factor of 0.6.

the rate constants at low temperature, an increase of the imaginary frequencies to 600i−680i cm^{-1} was required. The solid curves in Figure 8 show the results of the calculations for the best fit of the data for reaction 2a (reduction of the barrier by 0.9 kJ mol^{-1} and increase of the imaginary frequencies to 680 cm^{-1}). To obtain a better fit of the rate constants of reaction 2b, a somewhat smaller reduction of the barrier and a comparable increase in the imaginary frequency are required.

It should be noted, that a good agreement for reaction 2 can be achieved by reducing the barrier in reactions 2a,b by 2.5−3 kJ mol^{-1} within the modified TST even without invoking tunneling (i.e., using the harmonic imaginary frequencies which provide only a minor tunneling correction, ca. 27% at 200 K), with simultaneous reduction of the rate constant by a factor of 0.6. This is shown in the insert in Figure 8. As already mentioned, the curvatures of the Arrhenius plots alone are not sufficient to discriminate whether the negative temperature dependences are caused by negative energies of the transition states or by the enhanced tunneling. The barrier adjustment which is required to explain the experimental data for reactions 2 (2.5−3 kJ mol^{-1}) is within the expected ab initio accuracy. The scaling of the rate constants by a factor of 0.6 is, probably, also within the uncertainty of the transition state theory. In addition, it should be noted, that in reaction 2, in contrast to reaction 1, there is a very low frequency doubly degenerate vibration of the transition state (ca. 60 cm^{-1}), which is completely active at the temperatures of interest. It can be expected that such low frequency vibrations are highly anharmonic and are not calculated very reliably, which has direct impact on the accuracy of the partition function of the transition state.

One obvious difference between reactions 1 and 2 is that reaction 2 is strongly exothermic. One can then speculate that the abrupt drop in the PES profile after the saddle point due to the large exothermicity might be a reason for the barrier to be effectively thinner than expected based on the quadratic decomposition at the saddle point. However, this requires an accurate investigation of the PES in the region after the saddle point, which was beyond the scope of the current work.

It should be noted that the adjustments made for reaction 2 are not uncommon and could be considered as minor based on the status of the field. For example, in the most recent paper[25] for the reverse reaction 1a through the process of calibration the barrier energy was reduced by 8.8 kJ mol^{-1}, from the computed 18.8 kJ mol^{-1} to 10.0 kJ mol^{-1}. This substantially increases the thermal contribution, especially at low temperatures. Simultaneously, the imaginary frequency of the transition state was reduced from 1136i to 782i, which would substantially reduce tunneling. These two contributions are strongly correlated and could not be reliably separated based on the Arrhenius plot curvature alone. For reaction 1, there is a perfect agreement of our calculations with experiment at high temperatures (e.g., 500 K), where the tunneling corrections are relatively small (ca. 25% for reactions 1c,d). However, this agreement can not be an argument for the accuracy of the barrier energy calculations, since the calculated rate constants are based on the transition state theory, which has its own uncertainty. Tentatively, from the agreement observed at high temperatures, we are estimating that the probable absolute accuracy of the barrier height calculations is better than 1.7−3 kJ mol^{-1}.

Conclusions

Kinetic studies of the reaction of CH_3 with Cl_2 have been extended down to 188 K using the laser flash photolysis/photoionization mass spectrometry technique. The measurements indicate that below room temperature the activation energy is slightly negative, which changes to positive at higher temperatures. Similar behavior is found for the faster $CD_3 + Cl_2$ reaction which has been studied for the first time. These rate constants are quantitatively rationalized in terms of an ab initio potential energy surface with slight adjustment of the barrier height. Transition state theory and 1-D tunneling models were applied to the $CH_3 + Cl_2$ reaction, while a modified TST approach was applied to the CD_3 analogue where the adjusted top of the vibrationally adiabatic barrier is slightly below the energy of the reactants. Similar theoretical approaches were also used to analyze the CH_3 and CD_3 reactions with HCl and DCl whose barriers lie significantly above the energies of the reactants. Good agreement with the rate constants and kinetic isotope effects was obtained even in regimes where tunneling was significant.

Acknowledgment. A.J.E. and R.S.T. acknowledge support from the Biosciences and Environmental Research Council of the Academy of Finland and the Maj and Tor Nessling Foundation, and the NoNeCK (Nordic Network for Chemical Kinetics), and thank Mr. Harri Niemelä for help in conducting the experiments. P.M. thanks the R.A. Welch Foundation (Grant B-1174) and the UNT Faculty Research Fund for support. Computational facilities were provided at the UNT Research Cluster and purchased with funds from the National Science Foundation (Grant CHE-0342824).

References and Notes

(1) Blanksby, S. J.; Ellison, G. B. *Acc. Chem. Res.* **2003**, *36*, 255.
(2) Benson, S. W. *Thermochemical Kinetics*, 2nd ed.; Wiley: New York, 1976.
(3) Mozurkewich, M.; Benson, S. W. *J. Phys. Chem.* **1984**, *88*, 6429.

(4) Russell, J. J.; Seetula, J. A.; Gutman, D. *J. Am. Chem. Soc.* **1988**, *110*, 3092.
(5) Seetula, J. A.; Gutman, D. *J. Phys. Chem.* **1991**, *95*, 10688.
(6) Seetula, J. A. *Phys. Chem. Chem. Phys.* **2002**, *4*, 455.
(7) Seakins, P. W.; Pilling, M. J.; Niiranen, J. T.; Gutman, D.; Krasnoperov, L. N. *J. Phys. Chem.* **1992**, *96*, 9847.
(8) Nicovich, J. M.; Van Dijk, C. A.; Kreutter, K. D.; Wine, P. H. *J. Phys. Chem.* **1991**, *95*, 9890.
(9) Seetula, J. A. *J. Chem. Soc., Faraday Trans.* **1998**, *94*, 3561.
(10) Sheng, L.; Li, Z.-S.; Liu, J.-Y.; Sun, C.-C. *J. Chem. Phys.* **2003**, *119*, 10585.
(11) Krasnoperov, L. N.; Peng, J.; Marshall, P. *J. Phys. Chem. A* **2006**, *110*, 3110.
(12) Eskola, A. J.; Seetula, J. A.; Timonen, R. S. *Chem. Phys.* **2006**, *331*, 26.
(13) Gao, Y.; Alecu, I. M.; Hsieh, P.-C.; Morgan, B. P.; Marshall, P.; Krasnoperov, L. N. *J. Phys. Chem. A* **2006**, *110*, 6844.
(14) Eskola, A. J.; Timonen, R. S. *Phys. Chem. Chem. Phys.* **2003**, *5*, 2557.
(15) Lightfoot, P. D.; Kirwan, S. P.; Pilling, M. J. *J. Phys. Chem.* **1988**, *92*, 4938.
(16) Blais, N. C. *J. Chem. Phys.* **1983**, *79*, 1723.
(17) Donaldson, D. J.; Leone, S. R. *J. Chem. Phys.* **1986**, *85*, 817.
(18) Roxlo, C.; Mandl, A. *J. Appl. Phys.* **1980**, *51*, 2969.
(19) Truong, T. N.; Truhlar, D. G.; Baldridge, K. K.; Gordon, M. S.; Steckler, R. *J. Chem. Phys.* **1989**, *90*, 7137.
(20) Chen, Y.; Rauk, A.; Tschuikow-Roux, E. *J. Phys. Chem.* **1991**, *95*, 9900.
(21) Dobbs, K. D.; Dixon, D. A. *J. Phys. Chem.* **1994**, *98*, 12584.
(22) Duncan, W. T.; Truong, T. N. *J. Chem. Phys.* **1995**, *103*, 9642.
(23) Espinosa-Garcia, J.; Corchado, J. C. *J. Chem. Phys.* **1996**, *105*, 3517.
(24) Corchado, J. C.; Truhlar, D. G.; Espinosa-García, J. *J. Chem. Phys.* **2000**, *112*, 9375.
(25) Rangel, C.; Navarrete, M.; Corchado, J. C.; Espinosa-Garcia, J. *J. Chem. Phys.* **2006**, *124*, 124306.
(26) Martinez-Nunez, E.; Fernandez-Ramos, A.; Vazquez, S. A.; Rios, M. A. *Chem. Phys. Lett.* **2002**, *360*, 59.
(27) Yu, H.-G.; Nyman, G. *J. Chem. Phys.* **1999**, *111*, 6693.
(28) Boone, G. D.; Agyin, F.; Robichaud, D. J.; Tao, F.-M.; Hewitt, S. A. *J. Phys. Chem. A* **2001**, *105*, 1456.
(29) Bryukov, M. G.; Slagle, I. R.; Knyazev, V. D. *J. Phys. Chem. A* **2002**, *106*, 10532.
(30) Rudic, S.; Murray, C.; Harvey, J. N.; Orr-Ewing, A. J. *J. Chem. Phys.* **2004**, *120*, 186.
(31) Troya, D.; Millan, J.; Banos, I.; Gonzalez, M. *J. Chem. Phys.* **2002**, *117*, 5730.
(32) Garcia, E.; Sanchez, C.; Rodriguez, A.; Lagana, A. *Int. J. Quantum Chem.* **2006**, *106*, 623.
(33) Sellevag, S. R.; Nyman, G.; Nielsen, C. J. *J. Phys. Chem. A* **2006**, *110*, 141.
(34) Troya, D.; Weiss, P. J. *J. Chem. Phys.* **2006**, *124*, 074313.
(35) Castillo, J. F.; Aoiz, F. J.; Banares, L. *J. Chem. Phys.* **2006**, *125*, 124316.
(36) Banks, S. T.; Clary, D. C. *Phys. Chem. Chem. Phys.* **2007**, *9*, 933.
(37) Tirtowidjojo, M. M.; Colegrove, B. T.; Durant, J. L., Jr. *Ind. Eng. Chem. Res.* **1995**, *34*, 4202.
(38) Lee, J.; Bozzelli, J. W.; Sawerysyn, J. P. *Int. J. Chem. Kinet* **2000**, *32*, 548.
(39) Drougas, E.; Papayannis, D. K.; Kosmas, A. M. *J. Phys. Chem. A* **2002**, *106*, 6339.
(40) Frisch, M. J.; Trucks, G. W.; Schlegel, H. B.; Scuseria, G. E.; Robb, M. A.; Cheeseman, J. R.; Montgomery, J. A., Jr.; Vreven, T.; Kudin, K. N.; Burant, J. C.; Millam, J. M.; Iyengar, S. S.; Tomasi, J.; Barone, V.; Mennucci, B.; Cossi, M.; Scalmani, G.; Rega, N.; Petersson, G. A.; Nakatsuji, H.; Hada, M.; Ehara, M.; Toyota, K.; Fukuda, R.; Hasegawa, J.; Ishida, M.; Nakajima, T.; Honda, Y.; Kitao, O.; Nakai, H.; Klene, M.; Li, X.; Knox, J. E.; Hratchian, H. P.; Cross, J. B.; Adamo, C.; Jaramillo, J.; Gomperts, R.; Stratmann, R. E.; Yazyev, O.; Austin, A. J.; Cammi, R.; Pomelli, C.; Ochterski, J. W.; Ayala, P. Y.; Morokuma, K.; Voth, G. A.; Salvador, P.; Dannenberg, J. J.; Zakrzewski, V. G.; Dapprich, S.; Daniels, A. D.; Strain, M. C.; Farkas, O.; Malick, D. K.; Rabuck, A. D.; Raghavachari, K.; Foresman, J. B.; Ortiz, J. V.; Cui, Q.; Baboul, A. G.; Clifford, S.; Cioslowski, J.; Stefanov, B. B.; Liu, G.; Liashenko, A.; Piskorz, P.; Komaromi, I.; Martin, R. L.; Fox, D. J.; Keith, T.; Al-Laham, M. A.; Peng, C. Y.; Nanayakkara, A.; Challacombe, M.; Gill, P. M. W.; Johnson, B.; Chen, W.; Wong, M. W.; Gonzalez, C.; Pople, J. A. *Gaussian 03,* rev. B.04; Gaussian, Pittsburgh, 2003.
(41) NIST Computational Chemistry Comparison and Benchmark Database, NIST Standard Reference Database Number 101, Release 12; Johnson, R. D., III Ed. http://srdata.nist.gov/cccbdb, 2005.
(42) Schwartz, M.; Marshall, P. *J. Phys. Chem. A* **1999**, *104*, 7900.
(43) Schwartz, M.; Peebles, L. R.; Berry, R. J.; Marshall, P. *J. Chem. Phys.* **2003**, *118*, 557.
(44) Knowles, P. J.; Lindh, R.; Schutz, M.; Celani, P.; Korona, T.; Manby, F. R.; Rauhut, G.; Amos, R. D.; Bernhardsson, A.; Berning, A.; Cooper, D. L.; Deegan, M. J. O.; Dobbyn, A. J.; Eckert, F.; Hampel, C.; Hetzer, G.; Lloyd, A. W.; McNicholas, S. J.; Meyer, W.; Mura, M. E.; Nicklass, A.; Palmieri, P.; Pitzer, R.; Schumann, U.; Stoll, H.; Stone, A. J.; Tarroni, R.; Thorsteinsson, T. Molpro, rev. 2002.6, 2002.
(45) Woon, D. E.; Dunning, T. H., Jr. *J. Chem. Phys.* **1993**, *98*, 1358.
(46) Dunning, T. H., Jr.; Peterson, K. A.; Wilson, A. K. *J. Chem. Phys.* **2001**, *114*, 2944.
(47) Feller, D. *J. Chem. Phys.* **1992**, *96*, 6104.
(48) Herzberg, G. *Molecular Spectra and Molecular Structure. Vol. 2. Infrared and Raman Spectra of Polyatomic Molecules*; van Nostrand: New York, 1945; p 173.
(49) Kovalenko, L. J.; Leone, S. R. *J. Chem. Phys.* **1984**, *80*, 3656.
(50) Timonen, R. S.; Gutman, D. *J. Phys. Chem.* **1986**, *90*, 2987.
(51) Dobis, O.; Benson, S. W. *Z. Phys. Chem. (Munich)* **2001**, *215*, 283.
(52) Eskola, A. J.; Lozovsky, V.; Timonen, R. S. *Int. J. Chem. Kinet.* **2007**, *39*, 614.
(53) Evans, B. S.; Whittle, E. *Int. J. Chem. Kinet.* **1978**, 10.
(54) Timonen, R. S.; Seetula, J. A.; Gutman, D. *J. Phys. Chem.* **1990**, *94*, 3005.
(55) Timonen, R. S.; Russell, J. J.; Gutman, D. *Int. J. Chem. Kinet* **1986**, *18*, 1193.
(56) Ruscic, B.; Boggs, J. E.; Burcat, A.; Csaszar, A. G.; Demaison, J.; Janoschek, R.; Martin, J. M. L.; Morton, M. L.; Rossi, M. J.; Stanton, J. F.; Szalay, P. G.; Westmoreland, P. R.; Zabel, F.; Berces, T. *J. Phys. Chem. Ref. Data* **2005**, *34*, 573.
(57) Ruscic, B.; Pinzon, R. E.; Morton, M. L.; von Laszevski, G.; Bittner, S. J.; Nijsure, S. G.; Amin, K. A.; Minkoff, M.; Wagner, A. F. *J. Phys. Chem. A* **2004**, *108*, 9979.
(58) Wigner, E. *Z. Phys. Chem. (Leipzig)* **1932**, *B19*, 203.
(59) Quickert, K. A.; Le Roy, D. J. *J. Chem. Phys.* **1970**, *52*, 856.
(60) Nikitin, E. E. *Theory of Elementary Atomic and Molecular Processes in Gases*; Clarendon: Oxford, 1974.
(61) Bell, R. P. *Trans. Faraday Soc.* **1959**, *55*, 1.
(62) Skodje, R. T.; Truhlar, D. G. *J. Phys. Chem.* **1981**, *85*, 624.
(63) Johnston, H. S.; Rapp, D. *J. Am. Chem. Soc.* **1961**, *83*, 1.
(64) Johnston, H. S.; Heicklen, J. *J. Phys. Chem.* **1962**, *66*, 532.
(65) Fernandez-Ramos, A.; Truhlar, D. G. *J. Chem. Phys.* **2001**, *114*, 1491.

JP801999W